Synthesis and Characterization of $Li[Ni_{0.41}Li_{0.08}Mn_{0.51}]O_2$ Nanoplates for Li Battery Cathode Material

Jaephil Cho,*,† Yoojin Kim,† and Min Gyu Kim‡

Department of Applied Chemistry, Kumoh National Institute of Technology, Gumi 730-701, Korea, and Beamline Research Division, Pohang Accelerator Laboratory, Pohang University of Science and Technology, Pohang 790-784, Korea

Received: October 30, 2006; In Final Form: December 20, 2006

A hydrothermal method was used to prepare hexagonal layered $Li[Ni_{0.41}Li_{0.08}Mn_{0.51}]O_2$ nanoplates ($R\bar{3}m$) from a mixed solution of $Ni_{0.14}Mn_{0.86}O_2$ and $LiOH{\cdot}H_2O$ at 200 °C. In addition, an ion-exchange method was used at room temperature to obtain the $Ni_{0.45}Mn_{0.55}O_2$ precursor from $K_{0.32}MnO_2$-birnessite. Even though the spinel phase (*Fd*3*m*) was dominant at 150 °C, it was completely converted into a hexagonal layered phase at 200 °C in a condition of excess $LiOH{\cdot}H_2O$. The as-prepared $Li[Ni_{0.41}Li_{0.08}Mn_{0.51}]O_2$ consisted of stacked nanoplates with a plate thickness of approximately 7 nm. Ex situ X-ray diffraction and X-ray absorption spectroscopy were used to study electrochemical Li insertion and extraction reactions of $Li[Ni_{0.41}Li_{0.08}Mn_{0.51}]O_2$. The results show that the $Li[Ni_{0.41}Li_{0.08}Mn_{0.51}]O_2$ electrode operates predominately with the redox couple Ni^{2+}/Ni^{4+} between 4.8 and 2 V. On the other hand, the oxidation state of Mn was constant, even at a 4.8 V change, indicating that the 4+ state was predominant. The cycling behavior between 2 and 4.8 V at a current rate of 60 mA/g shows a maximum capacity of 200 mA h/g with only a slight capacity fading out to 30 cycles.

Introduction

Ni-based cathode materials have been widely used as coprecipitated $Ni_{1-x}M_x(OH)_2$ precursors for obtaining final products that have a lower cation-mixing ratio than products obtained by a conventional method with MO_2 and $Ni(OH)_2$ precursors.[1−11] However, the method using the coprecipitated powders requires a high firing temperature to obtain an ordered layered structure above 700 °C. Delmas et al. and other groups investigated ion-exchange reactions as well as extractions and insertions in layered transition metal oxide bronzes below 300 °C.[12−14] The products obtained by the methods of Delmas et al., however, have stoichiometries which differ from $LiMn_{1-x}M_xO_2$, contain water and protons, are of poor crystallinity, or do not maintain their structure during cycling. Armstrong et al. reported that anhydrous and stoichiometric $Li_{0.5}MnO_2$, which is analogous to $LiCoO_2$, was obtained by ion exchange from a $NaMnO_2$ precursor.[14,16] The $LiMnO_2$ was obtained by refluxing $NaMnO_2$ with an excess of LiCl or LiBr in $LiCoO_2$ and was obtained by ion exchange from a $NaMnO_2$ precursor.[15,16] The $LiMnO_2$ was obtained by refluxing $NaMnO_2$ with an excess of LiCl or LiBr in *n*-hexanol at 145−150 °C for 6−8 h. However, the layered $LiMnO_2$ had about 10% Mn^{3+} ions in the Li sites, and furthermore, during Li intercalation/deintercalation, the Mn atoms moved to adjacent layers and transformed to a spinel-like structure, which induced capacity fading.

Birnessite materials have reportedly been used as precursors for the synthesis of layered materials. Birnessite is a common manganese oxide; its two-dimensional layered structure consists of edge-shared MnO_6 octahedra with cations and water molecules that occupy the interlayer region.[17−22] The interlayer distance is typically 0.7 nm, and the birnessite formula is generally expressed as $A_xMnO_{2\pm x}(H_2O)_y$, where A typically represents an alkali metal cation; an ion-exchange method is generally used to study Na and K.[18] The average oxidation state of the mixed valence manganese normally falls between 3.6 and 3.8, which indicates a predominance of Mn^{4+} with minor amounts of Mn^{3+}.[19,21] Recently, Xu et al. obtained layered lithium-rich $Li_x[Li_yNi_nMn_m]O_2$ ($x \leq 1$, $y \leq 1/3$, $y + n + m \leq 1$) by using a hydrothermal treatment of the mixed layered $Ni(OH)_2$ and the birnessite-type manganese oxide in a concentrated LiOH solution at 200 °C. They reported a reversible capacity of 120 mA h/g between 2 and 4.2 V.[23]

We now report on the synthesis and characterization of layered hexagonal $Li[Ni_{0.41}Li_{0.08}Mn_{0.51}]O_2$ nanoplates derived from the use of layered $Ni_{0.45}Mn_{0.55}O_2$ materials obtained from an ion exchange with $K_{0.32}MnO_2$ birnessite at room temperature. The as-prepared nanoplates had a plate thickness of approximately 7 nm and showed highly reversible lithium-ion reactions without conversion to a spinel-like phase.

Experimental Section

Synthesis of $K_{0.32}MnO_2$ Birnessite. After slowly stirring a solution containing 3.16 g of $KMnO_4$ and 100 mL of distilled water for 30 min at 40 °C, we added the solution to 0.74 g of fumaric acid, thereby causing a rapid exothermic reaction which formed a brown gel. We annealed the gel at 400 °C for 6 h and then at 700 °C for 12 h. The resultant dark black powders were washed with water three times and vacuum dried at 200 °C overnight. By using inductively coupled plasma (ICP) mass spectrometry to analyze the sample, we confirmed the presence of $K_{0.32}MnO_2$ and an average Mn oxidation state of 3.67.

Synthesis of $Ni_{0.45}Mn_{0.55}O_2$. The as-prepared $K_{0.32}MnO_2$ birnessite was mixed with $NiCl_2{\cdot}6H_2O/K_{0.32}MnO_2$ with a weight

* Corresponding author. E-mail: jpcho@kumoh.ac.kr.
† Kumoh National Institute of Technology.
‡ Pohang University of Science and Technology.

10.1021/jp067116n CCC: $37.00
Published on Web 01/30/2007

ratio of 5:1 in 100 mL of distilled water. The mixture was stirred for 7 days at room temperature and finally washed with water four times in order to remove any residues that did not participate in the reaction.

Synthesis of $Li[Li_{0.08}Ni_{0.41}Mn_{0.51}]O_2$. After combining $LiOH\cdot H_2O$ and $Ni_{0.14}Mn_{0.86}O_2$ with weight ratios of 1:1, 2:1, 3:1, and 4:1, we mixed the combination in 50 mL of distilled water and transferred the mixture to an autoclave where it was maintained at 150 and 200 °C for 1−24 h. The as-prepared powders were rinsed with water and dried under vacuum at 120 °C. ICP analysis revealed that the sample with the molar ratio of 4:1 had a $Li_{1.15}Ni_{0.45}Mn_{0.55}O_{4.25}$ stoichiometry. Furthermore, this composition can be normalized as $Li[Li_{0.08}Ni_{0.41}Mn_{0.51}]O_2$.

Characterization. Powder X-ray diffraction (XRD) measurements were taken with a Rigaku DMax/2000PC with a Cu-target tube. We then used an ICP mass spectroscope (ICPS-1000IV, Shimadzu) to determine the metal contents. For the field-emission transition electron microscopy (TEM), which enabled us to investigate the microstructure of the samples, we used a JEOL 2100F microscope at 200 kV. In addition, Ni and Mn K-edge X-ray absorption spectra were obtained using a BL7C (electrochemistry) beamline at the Pohang Light Source, which is a third generation synchrotron radiation source in a 2.5 GeV storage ring with a ring current of 120−170 mA. A Si(111) double crystal monochromator was used to monochromatize the X-ray photon energy. Furthermore, by detuning the monochromator, we eliminated higher order harmonic contaminations and subsequently reduced the incident X-ray intensity by about 30%. Next, we monitored the incident X-ray intensity by using pure nitrogen gas-filled ionization chambers. The spectroscopic data was collected in a transmittance mode.

Electrochemical Characterization. Coin-type half-cell tests were conducted on samples which had different C rates between 2 and 4.8 V and the same 0.2 C rate for charging. We made the cathodes for the battery test cells from the active material (approximately 25 mg), the super P carbon black (MMM, Belgium), and a polyvinylidene fluoride binder (Solef) in a weight ratio of 80:10:10. Next, we prepared a cathode slurry by thoroughly mixing a *N*-methyl-2-pyrrolidene solution with the polyvinylidene fluoride, the carbon black, and the powdery cathode-active material. To prepare the electrodes, we coated Al foil with the cathode slurry and left it to dry at 130 °C for 20 min. The coin-type battery test cells (size 2016R), each of which contained a cathode, a Li metal anode, and a microporous polyethylene separator, were prepared in a helium-filled glovebox. The electrolyte used was 1.03 M $LiPF_6$ with ethylene carbonate/diethylene carbonate/ethyl-methyl carbonate (3/3/4 vol %, Cheil Ind. Korea).

Results and Discussion

Figure 1a shows XRD patterns of K-birnessite ($K_{0.32}MnO_2$) prepared by a sol−gel method. The pattern is dominated by two major peaks at 12° (002) and 22° (212) scattering angles, which are signatures of synthetic birnessite materials; the pattern also shows a preferred orientation along the *c*-axis. In addition, the very sharp peaks indicate the formation of highly crystalline materials. The pattern of the $K_{0.32}MnO_2$ can be indexed with hexagonal lattice constants, where the values of $a = 2.847(8)$ Å and $c = 21.535(9)$ Å are expanded to $a = 2.851(4)$ Å and $c = 21.616(8)$ Å after reaction with $NiCl_2\cdot 6H_2O$ (Figure 1b). The broadening of the two major peaks at approximately 12° and approximately 25.2° indicates increased disordering in the cations between the layers or indicates decreased crystallinity. Figure 1c,d,e shows XRD patterns of ion-exchanged $Ni_{0.45}Mn_{0.55}O_2$ before and after hydrothermal reactions with $LiOH\cdot H_2O$ at a variety of temperatures (150 °C and 200 °C) and weight ratios of $Ni_{0.45}Mn_{0.55}O_2$ to $LiOH\cdot H_2O$ (1:1, 1:2, and 1:4). In the case of the sample prepared at 150 °C for 4 h and a weight ratio of 1:1 ($LiOH/Ni_{0.45}Mn_{0.55}O_2$), the peaks assigned to the spinel phase with a cubic *Fd3m* space group are dominant though they contain a residual birnessite phase (Figure 1c); however, when both the hydrothermal temperature and the weight ratio were increased, a layered hexagonal phase with an $R\bar{3}m$ space group became dominant (Figure 1d,e). When the hydrothermal temperature was 200 °C for 4 h and the weight ratio was 4:1 ($LiOH\cdot H_2O/Ni_{0.45}Mn_{0.55}O_2$), all of the peaks could

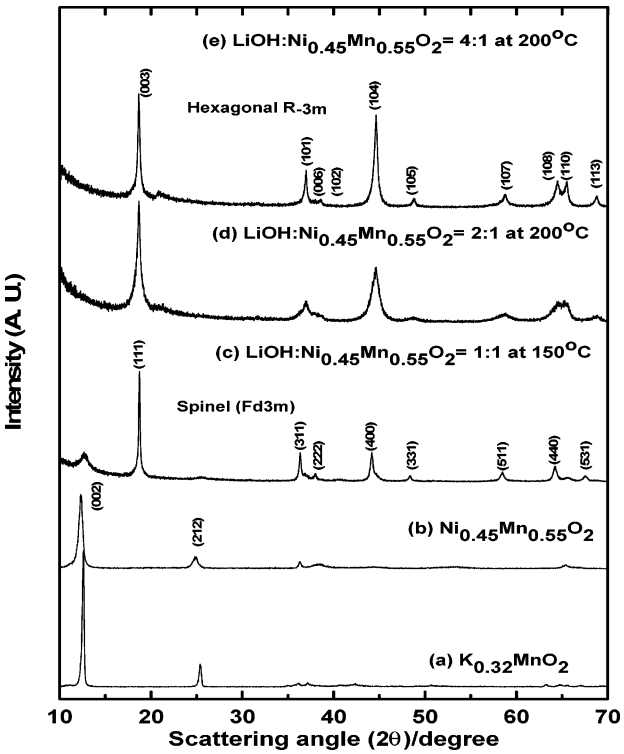

Figure 1. XRD patterns of (a) $K_{0.32}MnO_2$, (b) $Ni_{0.45}Mn_{0.55}O_2$, and (c−e) as-prepared samples from a hydrothermal method in a mixed solution of $LiOH\cdot H_2O$ and $Ni_{0.45}Mn_{055}O_2$ with a weight ratio of 1:1, 2:1, and 4:1.

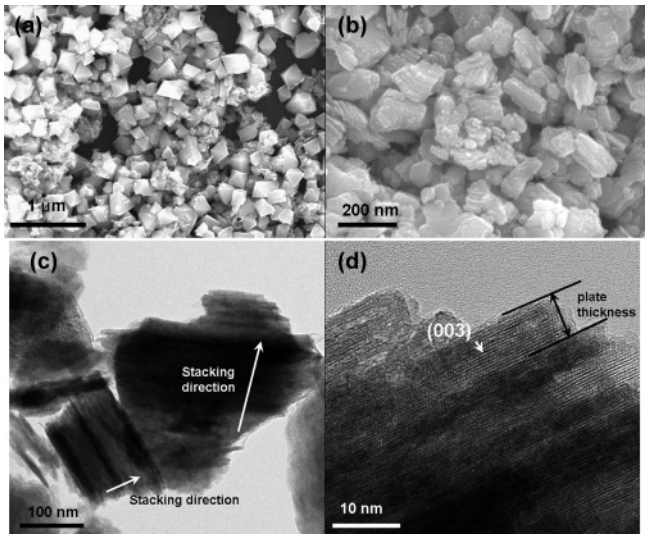

Figure 2. SEM and TEM images of samples prepared at (a) 150 °C with a weight ratio of 1:1 and at (b−d) 200 °C with a ratio of 4:1 ($LiOH\cdot H_2O/Ni_{0.45}Mn_{0.55}O_2$).

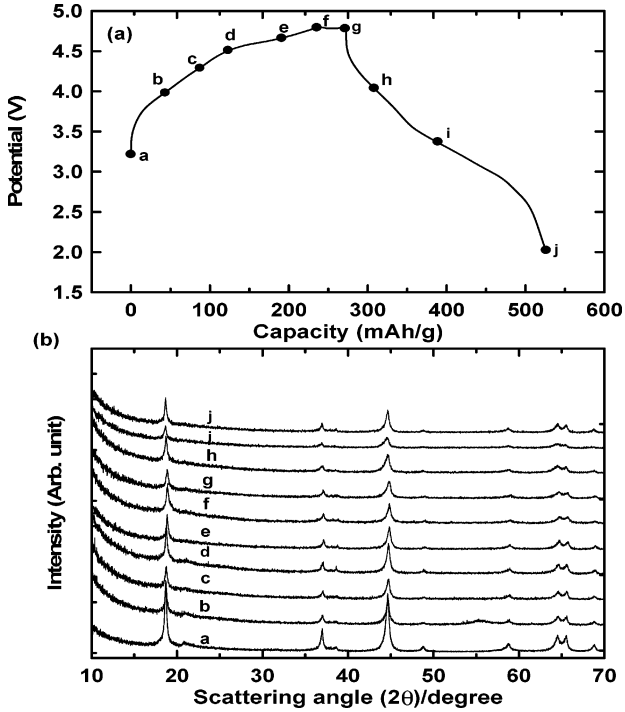

Figure 3. Voltage profiles of the sample between 2 and 4.8 V at a rate of 0.01 C and corresponding ex situ XRD patterns.

be assigned to a hexagonal layered phase (Figure 1e). We attribute the small XRD peaks between 20° and 25° to the superlattice ordering of Li and Mn in the layers that contained transition metals. These superlattice peaks are observable in XRD patterns of Li_2MnO_3-based oxides.[24−26]

Figure 2 shows scanning electron microscopy (SEM) and TEM images of the samples prepared at 150 °C (a) with a weight ratio of 1:1 and at 200 °C (b−d) with a weight ratio of 4:1 ($LiOH{\cdot}H_2O/Ni_{0.45}Mn_{0.55}O_2$). The first sample clearly shows a typical octahedral spinel phase with a [111] plane direction. After hydrothermal reactions at 200 °C, the morphology is completely transformed into stacked nanoplates with a particle size of about 200 nm. The high-resolution image of Figure 2c in Figure 2d clearly shows the stacked nanoplate with a thickness of approximately 7 nm along the *c*-axis, as well as a lattice fringe along the (003) plane with a *d*-spacing value of 0.46 Å. Figure 3, which shows the voltage profiles of the sample between 2 and 4.8 V at a rate of 0.01 C and ex situ XRD patterns at different charge and discharge voltages, demonstrates how the initial hexagonal layer structure is maintained.

Figure 4 depicts a plot of lattice constants *a* and *c* along with the volume expansion of the cathode at the designated charge and discharged potentials, identical to Figure 3. Up to the beginning of the 4.8 V plateau, the *c*-axis increases. However, the *c*-axis decreases rapidly at the end of the plateau when the last lithium ions are removed from the lithium layers.[27] The *a*-axis presumably decreases because the radius of Ni^{4+} is smaller than that of Ni^{2+}. During the lithium extraction, the oxygen lattice contracts in response to the increase in the average oxidation state of the nickel, and there is a decrease in the average bond length of Ni−O. Once the 4.8 V plateau is reached, the *a*-axis remains approximately constant, suggesting that the transition metal oxidation state does not change during further charging. This constant value of the *a*-axis, which is related to the removal of oxygen atoms from the lattice, should be accompanied by the removal of the lithium; moreover, the expelled oxygen may react with the electrolyte that is responsible for the irreversible capacity.[28,29]

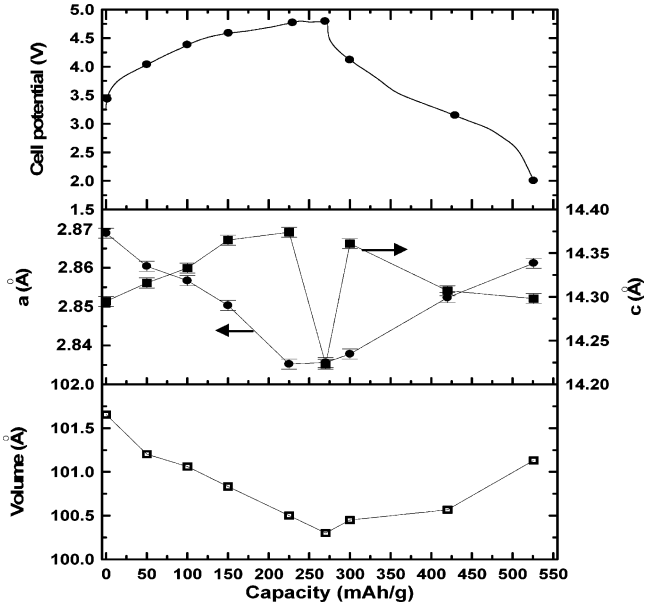

Figure 4. Plots of lattice constants *a* and *c*, along with the volume expansion of the cathode at designated charge and discharged potentials, identical to Figure 3.

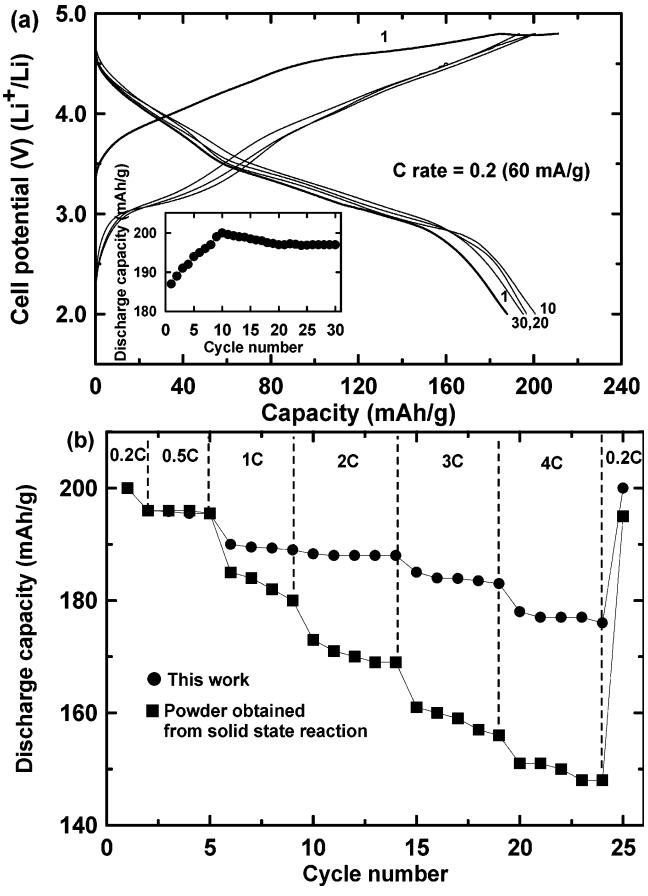

Figure 5. (a) Voltage profiles of the $Li[Ni_{0.41}Li_{0.08}Mn_{0.51}]O_2$ cathode after 1, 10, 20, and 30 cycles at a rate of 0.2 C (= 40 mA/g, inset is a plot of the discharge capacity as a function of the cycle number); (b) the rate capabilities of the nanoplates and powder prepared at 750 °C according to ref 26 at 0.2, 0.5, 1, 2, 3, and 4 C rates. The charge rate was fixed at 0.2 C (= 60 mA/g).

Figure 5a shows the voltage profiles of the $Li[Ni_{0.41}Li_{0.08}Mn_{0.51}]O_2$ cathode after 1, 10, 20, and 30 cycles. The irreversible capacity ratio after the first cycle is 11%, representing a charge capacity of 200 mA h/g and a discharge capacity of 187 mA

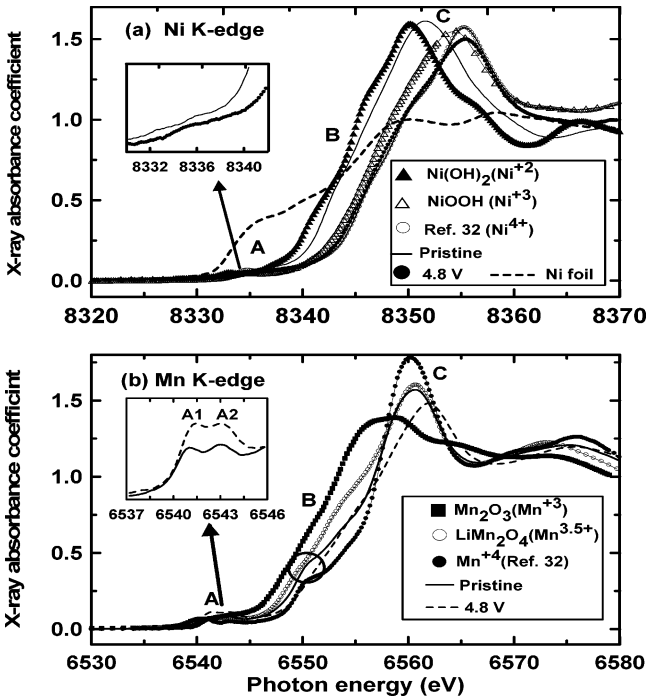

Figure 6. Comparison of Ni and Mn K-edge XANES spectra of the pristine sample (before charging) and after charging to 4.8 V, in relation to the references.

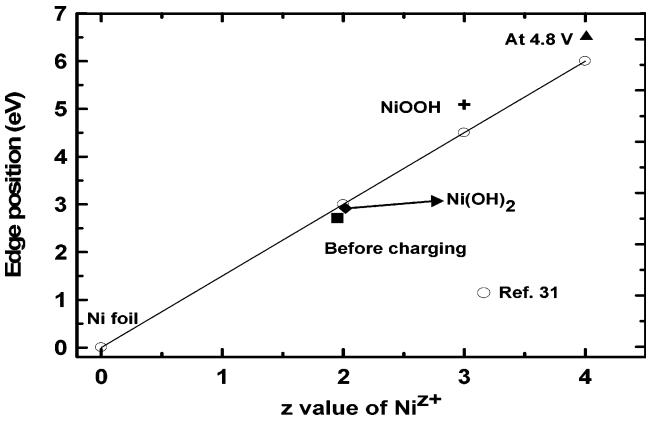

Figure 7. Relation between the oxidation state of Ni ions and the edge position, with respect to the data reported in ref 31.

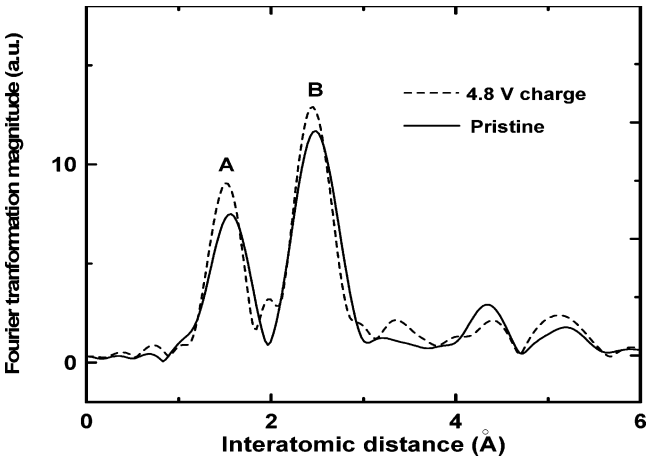

Figure 8. FT magnitude of Ni K-edge EXAFS spectra for the samples before charging and after charging to 4.8 V.

h/g. The discharge capacity reached a maximum after 10 cycles and then diminished slowly before reaching a value of 197 mA h/g after 30 cycles. The inset of Figure 5a shows the discharge capacity as a function of the life cycle: the capacity was 200 mA h/g after 10 cycles and then diminished by 1% up to 30 cycles. Because of the unique morphology of the cathode nanoplates, we can expect faster lithium-ion diffusivity into and out of the nanoplate layer. Hence, we prepared the cathode powders with the same stoichiometry as the reference at 750 °C, and they had a similar particle morphology to that shown in ref 30 (that is, spherical, with a particle size of about 13 μm). Next, we compared the rate capability of these powders with that of the nanoplates. As can be seen in Figure 5b, the capacity loss of the nanoplates is much smaller than that of the samples prepared at 750 °C at higher C rates. For instance, the capacity of the nanoplates is 184 mA h/g, whereas the capacity of the sample prepared at 750 °C is 160 mA h/g at a 3 C rate. Furthermore, in contrast to the reference sample, the capacity of our sample was fully restored to 200 mA h/g after extended high-rate cycling.

To obtain detailed information on the oxidation state of the samples, we compared Ni and Mn K-edge X-ray absorption near-edge spectroscopy (XANES) spectra of the pristine (before charging) sample and a sample after charging to 4.8 V with reference spectra (Figure 6a,b). The Ni K-edge peak feature for the pristine sample shows that the Ni^{2+} clearly shifts toward the higher energy region after charging to 4.8 V with respect to those of lower oxidative Ni reference materials. The peak position is quite similar to a peak that corresponds to the Ni^{4+} state.

As shown in Figure 7, the chemical variation of the Ni ion can be discussed in terms of the relation between the oxidation states of the Ni ion and the edge position. Our results agree well with those of an earlier report.[31] Furthermore, the sample that exists in the Ni^{2+} state before the occurrence of any charging is oxidized to the Ni^{4+} state after 4.8 V charging. A weak absorption peak, A, for the 1s → 3d quadrupole-allowed transition, appeared at about 8333 eV with Ni 3d−4p orbital mixing by means of the structural distortion of the NiO_6 octahedra. Two absorption peaks for the 1s → 4p dipole-allowed transitions, with and without the shakedown process of the ligand-to-metal charge transfer, were observed at about 8342 eV (Figure 6a, peak B) and 8351 eV (Figure 6a, peak C), respectively.[32] Furthermore, because of the local structural distortion around the NiO_6 octahedra during the Li-ion extraction, there was a systematic decrease in the peak intensity for the ligand-to-metal charge-transfer process, followed by a decrease in the Ni−O bond covalency. The increase in the $Ni^{4+}-O^{2-}$ character in the 4.8 V charged state is closely associated with the transfer of the hole state in the oxygen 2p band to the Ni atomic site.

As shown in Figure 6b, a weak double-peak (A1 and A2) structure is visible in the pre-edge region, A, of the Mn K-edge XANES spectra. Peaks A1 and A2 are assigned to the quadruple-allowed 1s → 3d (t_{eg}) transition and the 1s → 3d (e_g) transition, respectively. The experimental spectra of the pristine sample (before charging) are consistent with the octahedral or near-octahedral coordination of manganese. Furthermore, the intermediate bump at 6552 eV (marked with a solid circle) is prominent in the pristine sample. The magnitude of this bump is related to the connectivity between the MnO_6 octahedra in the structure. After the sample was charged to 4.8 V, the shape of the near-edge spectrum in region B and region C changed significantly. This result does not represent an increase of the Mn oxidation state because Mn^{4+} normally cannot be oxidized beyond the 4+ oxidation state. Rather, the change can be explained by a possible rearrangement of the Mn local structure.

The intermediate bump almost disappears, which is consistent with a disordered arrangement of the MnO_6 octahedra in the sample.

Besides discussing the oxidation state in relation to the XANES spectra, we quantitatively analyzed the local structure variations of the sample by using extended X-ray absorption fine structure (EXAFS) spectra and by focusing on the specified local structure around each central atom. Figure 8 shows the Fourier transform (FT) magnitudes for the Ni K-edge k^3-weighted spectra of the pristine samples charged at 4.8 V. All of the FTs show typical FT features for an $R\bar{3}m$ layered structure in which the Ni cations form well-distributed octahedral layers. The FT peaks A and B correspond to the six nearest neighbors of the coordinated oxygen around the central Ni atom and six coordinated Ni atoms in the next edge-shared octahedral site. The result is consistent with that of the ex situ XRD patterns described above. After charging the sample to 4.8 V, FT peak B shifts slightly to the lower $Ni^{2+}-O$ bond distance, that is, from approximately 2.04 Å to 1.9 Å (for a phase correction factor of approximately 0.44 Å). On the basis of the effective ionic radii determined by Shannon and Prewitt, we considered the oxidation states of the Ni ion for two discrete bond distances to be Ni^{2+} and Ni^{4+}, where the ionic radii can be obtained for a given coordination number.[33] This estimate is consistent with the XANES result.

Conclusion

After preparing $Li[Ni_{0.41}Li_{0.08}Mn_{0.51}]O_2$ nanoplates from $K_{0.32}$-MnO_2 birnessite at low temperature, we demonstrated a new way of obtaining a highly ordered layered structure. The results of electrochemical lithium extraction in $Li[Ni_{0.41}Li_{0.08}Mn_{0.51}]$-$O_2$, for up to 4.8 V, suggest that the charge is compensated by the electronic transition between Ni^{2+} and Ni^{4+}. However, the oxidation state of Mn remains constant at predominantly 4+. Furthermore, the electrochemical cycling results show a maximum reversible capacity of 200 mA h/g between 2 and 4.8 V with little capacity loss after 30 cycles. This new synthetic method can be applied to the insertion of other transition metals such as Co and Fe ions.

Acknowledgment. We are grateful to Pohang Light Source (PLS) for allowing us to conduct XAS measurements. This study was supported by University ITRC center project.

References and Notes

(1) Jeong, J. W.; Kang, S. G. *J. Power Sources* **2003**, *123*, 75.
(2) Rossen, E.; Jones, C. D. W.; Dahn, J. R. *Solid State Ionics* **1992**, *57*, 311.
(3) Rougier, A.; Gravereau, P.; Delmas, C. *J. Electrochem. Soc.* **1996**, *143*, 1168.
(4) Spahr, M. E.; Novak, P.; Schnyder, B.; Hass, O.; Nesper, R. *J. Electrochem. Soc.* **1998**, *145*, 1113.
(5) Yoshio, M.; Todorov, Y.; Yamoto, K.; Noguchi, H.; Itoh, J.; Okada, M.; Mouri, T. *J. Power Sources* **1998**, *74*, 64.
(6) Schougaard, S. B.; Breger, J.; Jiang, M.; Grey, C. P.; Goodenough, J. B. *Adv. Mater. (Weinheim, Ger.)* **2006**, *18*, 905.
(7) Cho, J.; Jung, H.; Park, Y.; Kim, G.; Lim, H. S. *J. Electrochem. Soc.* **2000**, *147*, 15.
(8) Cho, J.; Kim, G.; Lim, H. S. *J. Electrochem. Soc.* **1999**, *146*, 3571.
(9) Cho, J. *Chem. Mater.* **2001**, *13*, 4537.
(10) Park, S. H.; Park, K. S.; Sun, Y. K.; Nahm, K. S.; Lee, Y. S.; Yoshio, M. *Electrochim. Acta* **2001**, *46*, 1215.
(11) Kim, G. H.; Myung, S. T.; Bang, H. J.; Prakash, J.; Sun, Y.-K. *Electrochem. Solid-State Lett.* **2004**, *7*, A477.
(12) Delmas, C.; Braconnoer, J.-J.; Maazaz, A.; Hagenmuller, P. *Rev. Chim. Miner.* **1982**, *19*, 343.
(13) Rossouw, M. H.; Liles, D. C.; Thackeray, M. M. *J. Solid State Chem.* **1993**, *104*, 464.
(14) Armstrong, A. R.; Bruce, P. G. *Nature* **1996**, *381*, 499.
(15) Capitaine, F.; Gravereau, P.; Delmas, C. *Solid State Ionics* **1996**, *89*, 197.
(16) Bruce, P. G.; Armstrong, A. R.; Gitzendanner, R. L. *J. Mater. Chem.* **1996**, *9*, 193.
(17) Chen, R.; Zavalij, P.; Whittingham, M. S. *Chem. Mater.* **1996**, *8*, 1275.
(18) Ching, S.; Petrovay, D. J.; Jorgensen, M. L.; Suib, S. L. *Inorg. Chem.* **1997**, *36*, 883.
(19) Ching, S.; Landrigan, J. A.; Jorgensen, M. L. *Chem. Mater.* **1995**, *7*, 1604.
(20) Le Goff, P.; Baffier, N.; Bach, S.; Perei-Ramos, J. P. *Mater. Res. Bull.* **1996**, *31*, 63.
(21) Shen, Y.-F.; Suib, S. L.; O'Young, C.-L. *J. Am. Chem. Soc.* **1994**, *116*, 11020.
(22) Tsuda, M.; Arai, H.; Sakurai, Y. *J. Power Sources* **2002**, *52*−*56*, 110.
(23) Xu, Y.; Feng, Q.; Kajiyoshi, K.; Yanagisawa, K.; Yang, X.; Makita, Y.; Kasaishi, S.; Ooi, K. *Chem. Mater.* **2002**, *14*, 3844.
(24) Park, Y. J.; Hong, Y.-S.; Wu, X.; Kim, M. G.; Ryu, K. S.; Chang, S. H. *J. Electrochem. Soc.* **2004**, *151*, A720.
(25) Ammundsen, B.; Paulsen, J. *Adv. Mater.* **2001**, *13*, 943.
(26) Hong, Y. S.; Park, Y. J.; Wu, X.; Ryu, K. S.; Chang, S. H. *Electrochem. Solid State Lett.* **2003**, *6*, A166.
(27) Amatucci, G. G.; Tarascon, J. M.; Klein, L. C. *J. Electrochem. Soc.* **1996**, *143*, 1114.
(28) Lu, Z.; Dahn, J. R. *J. Electrochem. Soc.* **2002**, *149*, A815.
(29) Armstrong, A. R.; Holzapfel, M.; Novak, P.; Johnson, C. S.; Kang, S.-H.; Thackery, M. M.; Bruce, P. G. *J. Am. Chem. Soc.* **2006**, *128*, 8694.
(30) Kim, J.; Hong, Y.; Ryu, K. S.; Kim, M. G.; Cho, J. *Electrochem. Solid State Lett.* **2006**, *9*, A19.
(31) Montoro, L. A.; Abbate, A.; Almeida, E. C.; Rosolen, M. *J. Electrochem. Soc.* **2000**, *147*, 3729.
(32) Kim, M.-G.; Shin, H. J.; Kim, J.-H.; Park, S.-H.; Sun, Y.-K. *J. Electrochem. Soc.* **2005**, *152*, A1320.
(33) Shannon, R. D.; Prewitt, C. T. *Acta Crystallogr., Sect. A.: Cryst. Phys., Diffr., Theor. Gen. Crystallogr.* **1976**, *A32*, 751.